Critical exponents of colloid particles in bulk and confinement

Helge Neitsch[1, a)] and Sabine H. L. Klapp[1, b)]

Institut für Theoretische Physik, Sekr. EW 7-1, Fakultät II für Mathematik und Naturwissenschaften, TU Berlin, Hardenbergstraße 36, D-10623 Berlin

Using grand canonical Monte Carlo simulations, we investigate the percolation behavior of a square well fluid with an ultra-short range of attraction in three dimension (3D) and in confined geometry. The latter is defined through two parallel and structureless walls (slit-pore). We focus on temperatures above the critical temperature of the (metastable) condensation transition of the 3D system. Investigating a broad range of systems sizes, we first determine the percolation thresholds, i. e., the critical packing fraction for percolation η_c. For the slit-pore systems, η_c is found to vary with the wall separation L_z in a continuous but non-monotonic way, $\eta_c(L_z \to \infty) = \eta_c^{3D}$. We also report results for critical exponents of the percolation transition, specifically, the exponent ν of the correlation length ξ and the two fisher exponents τ and σ of the cluster-size distribution. These exponents are obtained from a finite-size analysis involving the cluster-size distribution and the radii of gyration distribution at the percolation threshold. Within the accuracy of our simulations, the values of the critical exponents of our 3D system are comparable to those of 3D random percolation theory. For narrow slit-pores, the estimated exponents are found to be close to those obtained from the random percolation theory in two dimensions.

[a)]Electronic mail: helge.neitsch@physik.tu-berlin.de

[b)]Electronic mail: klapp@physik.tu-berlin.de

I. INTRODUCTION

Percolation is a geometrical transition, in which interacting units such as the particles in a fluid, the spins on a lattice, or the nodes of a network spontaneously form system-spanning clusters termed the "percolated phase".[1] In contrast the units are distributed homogeneously or form isolated clusters of finite size in the non-percolated phase.

In this publication we focus on continuous systems, where percolation was originally discussed as a phenomenon in the context of flow through porous media. Later, the statistical theory of percolation has been used to understand the critical behavior of fluid (Fisher's droplet model)[2,3], particularly the divergence of the correlation length and the critical exponents characterizing the behavior close to the critical point. Indeed, it is well known that percolation obeys concepts of universality and scaling, similar to second-order thermodynamic phase transitions.[4] This includes the universality class of the so-called random percolation, which is assumed to apply to continuous systems such as fluids.

More recent (experimental and theoretical) research on continuous percolation often involves colloidal suspensions. One important topic in this area concerns the percolation of rod-like colloids, prominent examples being carbon nanotubes and other carbon-based particles[5–8]. From an applicational point of view the underlying idea is that the percolated network leads to lightweight materials with strongly enhanced mechanical stability and electrical (and/or thermal) conductivity. Another main topic, which concerns particularly complex colloidal mixtures[9,10] and colloids with directional interactions[11–13], is the intimate relation between percolation and the formation of a physical gel, which is a state in which particles are connected via bonds of limited lifetime. It is now well established that such colloidal gels, which are characterized through a very specific dynamic behavior, can form at extremely low packing fractions. Note, however, that gelation is a phenomenon which normally occurs for very strong coupling conditions, i. e., at temperatures far below those related to the vapor-liquid critical point (if the latter exists at all).

In the present study we are interested in the characteristics of the percolation transition at moderate (supercritical) temperatures, focusing on a system of spherical colloids with attractive interactions. Specifically, we aim to determine the percolation threshold, the scaling behavior and the related critical exponents. We consider both, three-dimensional (3D) systems and systems in slit-pore geometries which are infinite in only two dimensions

(2D). Our investigations are based on grand-canonical Monte Carlo (GCMC) computer simulations combined with a finite-size scaling analysis.

Our study is partially motivated by a series of recent Monte Carlo (MC) results by Nezbeda and coworkers.[14–16]These authors investigated the percolation in the corresponding supercritical regimes of various 3D (bulk) continuous model systems, differing in the precise form of the interaction potential.[15] Using different geometric cluster definitions and spanning rules, they found perfect scaling behavior for all systems investigated. However, the critical exponents turned out to be strongly dependent on the specific interaction potential and the temperature. This obviously contradicts the expectation that the percolation transition in these systems is universal. Indeed, in ideal random percolation the critical exponents and scaling functions only depend on the dimensionality and the symmetries of the system.[1]

Here we present results from a GCMC study involving colloids with an ultra-short range of attraction, modeled by a square-well potential with an attraction width of only four percent of the colloidal diameter. This is considerably smaller than the range of fifty percent studied in Ref. 15. Interestingly, our GCMC results for the 3D case do indicate *universality* of the exponents in the sense that they do not depend on the temperature in the range considered. The exponents do, however, depend on the spatial dimensionality, consistent with the predictions from random percolation theory.

We note that our model is by no means artificial. Indeed, colloids with ultra-short ranged interactions can be experimentally realized by adding small, non-adsorbing polymers to the colloidal solution, yielding short-range, attractive depletion interactions of tunable range[17]. Another, recently studied example (where the justification of the ultra-short ranged square-well model has actually been checked using scattering data) are silica nanoparticles with added lysozyme[18].

This paper is organized as follows. In Sec. II we introduce the model and discuss its bulk phase diagram. Numerical details of the GCMC simulations are described in Sec. III. In Sec. IV we present our numerical results for the percolation thresholds and critical exponents of the bulk and slit-pore systems. Specifically, we consider the exponents of the correlation length, the cluster size distribution, and the radius of gyration. In Sec. IV C we finally present results for the confinement-induced shift of the percolation threshold, and we provide a simple theory based on scaling arguments to describe this shift. We close this paper with the conclusions in Sec. V.

II. MODEL

In our colloidal model system, the particles interact via an attractive square-well (SW) potential defined as

$$u_{\mathrm{SW}}(\boldsymbol{r}_{ij}) = \begin{cases} \infty, & r_{ij} < \sigma \\ -\epsilon, & \sigma \leq r_{ij} < \lambda \\ 0, & \lambda \leq r_{ij} \end{cases} . \tag{1}$$

In Eq. (1) $r_{ij} = |\boldsymbol{r}_{ij}| = |\boldsymbol{r}_i - \boldsymbol{r}_j|$ is the particle distance, σ is the hard-core diameter, $\epsilon > 0$ is the strength of the attraction and λ determines the range of this attraction, i. e., $\lambda > \sigma$. Here we choose a value $\lambda = 1.04\sigma$, corresponding to a system with an ultra-short range of attraction.

The SW model with ultra-short ranged attraction has attracted growing attention, since it is known to be a simple but adequate model for colloidal suspensions. Indeed, short-ranged attractive colloids can be realized experimentally by adding small non-adsorbing polymers to the colloidal solution. This creates a depletion effect leading to an effective attraction between the colloids. To screen the remaining (attractive) Van der Waals interactions between the colloids, one chooses a solvent of similar dielectric permittivity.[9,19,20] If the difference in the length scales between the polymers and the colloids is sufficiently large, the degrees of freedom associated with the polymers can be "integrated out" of the theoretical description. The remaining implicit effect is an effective short-ranged attraction between the colloids due to depletion interactions.[21] Regarding the actual value of λ, we note that for values $\lambda \lesssim 1.25\sigma$ the stable liquid phase disappears and a typical colloidal phase diagram involving only a fluid and a solid phase arises.[22]

We consider our colloidal model in three dimensions (bulk) and in slit-pore geometries. The latter are realized by two plane-parallel structureless walls, which are parallel to the x-y-plane of the coordinate system and located at $\pm L_z/2$. The wall-particle interaction is modeled via

$$u_{\mathrm{wall}}(d) = \begin{cases} \infty, & d < \sigma/2 \\ 0, & d \geq \sigma/2 \end{cases} \tag{2}$$

with the particle-wall distance d. Thus, the slit-pore-particle interaction is given by

$$u_{\mathrm{slit}}(\boldsymbol{r}_i) = u_{\mathrm{wall}}(L_z/2 + z_i) + u_{\mathrm{wall}}(L_z/2 - z_i)) \tag{3}$$

where z_i is the z-component of the center of mass position $\boldsymbol{r}_i$ of the ith particle. Such a purely repulsive colloid-wall potential can be realized experimentally by using surface structures like a polymer-coated brush, which is penetrable for the polymers but not for the colloids.[20,23]

Recent research has shown that short-ranged systems, such as the present SW model, exhibit thermodynamic properties which are insensitive to the specific shape of the interaction potential and approximately fulfill an extended law of corresponding states.[24–26] This will be useful to derive a rough draft of the bulk phase diagram of our system. To this end we first consider a limit case of the SW model, the Baxter model, which is also referred to as the adhesive spheres (AHS) model. Within this model the limits $\lambda \to \sigma$ and $-\epsilon \to -\infty$ are determined while keeping the ratio of the second virial coefficient of the AHS model, B_2^{AHS}, to the second virial coefficient of the hard sphere system (HS), $B_2^{\mathrm{HS}} = 4\pi\sigma^3/3$, constant, that is

$$\frac{B_2^{\mathrm{AHS}}}{B_2^{\mathrm{HS}}} = 4\tau^{\mathrm{AHS}} - 1 \stackrel{!}{=} const. \tag{4}$$

Equation (4) defines the stickiness parameter τ^{AHS}, which describes to which extend the AHS particles tend to glue together. Hence τ^{AHS} acts as an effective dimensionless temperature in the Baxter model.

The Baxter model has been extensively investigated both by theory and by simulation.[26–28] Within the fluid phase regime it exhibits two types of phase transitions, namely a percolation transition and a vapor-liquid (vl) condensation transition. The critical parameters of the latter have been determined with very high accuracy using GCMC simulations. Their values are $\rho_{c,\mathrm{vl}}^{\mathrm{AHS}} = 0.508(10)/\sigma^3$ (the critical particle density) and $\tau_{c,\mathrm{vl}}^{\mathrm{AHS}} = 0.1133(5)$ (the critical temperature). Based on these values, we can now estimate the locus of the vapor-liquid critical point in the present square-well system. The first assumption is that the packing fraction $\eta = \pi\sigma^3\rho/6$ associated to the critical density remains constant, when we replace σ, which corresponds to the average distance of two bonded particles in AHS system, with the corresponding average distance d_{av} in the SW system. In other words, we require[26,29]

$$\rho_{c,\mathrm{vl}} d_{\mathrm{av}}^3 \stackrel{!}{=} \rho_{c,\mathrm{vl}}^{\mathrm{AHS}} \sigma^3. \tag{5}$$

For the present model, see Eq. (1), we have $d_{\mathrm{av}} = \sigma + (\lambda - \sigma)/2$. Inserting this into Eq. (5), one obtains

$$\rho_{c,\mathrm{vl}} = \frac{\sigma^3 \rho_{c,\mathrm{vl}}^{\mathrm{AHS}}}{(\sigma + (\lambda - \sigma)/2)^3}. \tag{6}$$

To estimate the critical temperature, we apply the Noro-Frenkel law of corresponding states. It states that two systems which are similar in nature by having both a hard-core repulsion and an (ultra-)short-ranged attraction have equal reduced second virial coefficients, provided we reduce with B_2^{HS} close to the critical temperatures in each case.[24] This allows us to apply a mapping of the phase diagram of one of those systems to the other. Taking the AHS as the reference system and equating its reduced second virial coefficient with the reduced second virial coefficient of a short-ranged SW model yields

$$\frac{B_2^{\mathrm{AHS}}}{B_2^{\mathrm{HS}}} = 4\tau^{\mathrm{AHS}} - 1 \stackrel{!}{=} \frac{B_2^{\mathrm{SW}}}{B_2^{\mathrm{HS}}} = 1 - ((\lambda/\sigma)^3 - 1)(e^{1/T^*} - 1). \tag{7}$$

In Eq. (7) we introduced the reduced temperature $T^* = k_B T/\epsilon$. Solving Eq. (7) with respect to T^* we obtain

$$T^* = \left[\ln\left(1 + \frac{1}{4\tau^{\mathrm{AHS}}\left((2-\lambda/\sigma)^{-3} - 1\right)}\right)\right]^{-1}. \tag{8}$$

Based on Eqs. (6) and (8), we can estimate the critical parameters of the present model by inserting the known values for $\rho_{c,\mathrm{vl}}^{\mathrm{AHS}}$ and $\tau_{c,\mathrm{vl}}^{\mathrm{AHS}}$, respectively. This yields

$$\eta_{c,\mathrm{vl}} = 0.250(5),\ T_{c,\mathrm{vl}}^* = 0.346(5)$$

where $\eta_{c,\mathrm{vl}}$ is the critical packing fraction of the vapor-liquid condensation transition.

In addition to determining the critical point, we may use the mapping procedure described above to obtain an estimate of the full fluid-fluid coexistence curve (binodal), as reviewed in Ref. 30. To this end, we apply Eq. (6) and Eq. (8) to GCMC data for the binodal taken from Fig. 3 of Ref. 31. Moreover, from integral equation studies[32] of a SW system with $\lambda = 1.03\sigma$, the fluid-solid coexistence line is known (see Fig. 9 of Ref. 32). Taking their data and applying the mapping procedure again, we obtain an estimate of the fluid branch of the fluid-solid coexistence line in our system. Finally, we also mapped the data of the percolation threshold given in Ref. 31.

Since we are partly far away from the critical point during such mapping, some doubts are appropriate regarding the justification of that strategy. Nevertheless, the mapping results give a first idea of the phase diagram of the present system. A summary of the results of these mapping procedures is given in Fig. 1. Included in this figure are our present GCMC results for the bulk percolation thresholds, which will be discussed in more detail in Sec. IV. The resulting percolation line divides the phase diagram into two regions characterized by

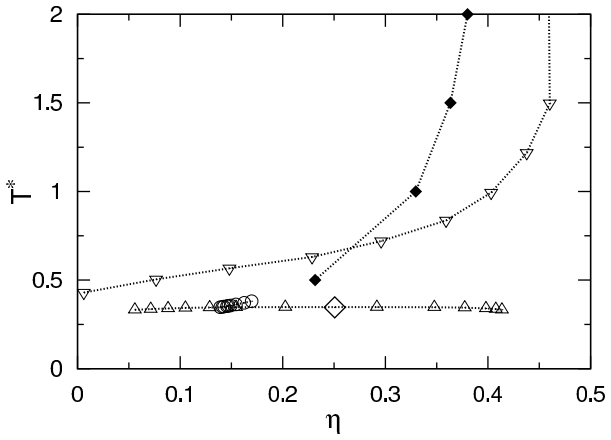

Figure 1. Estimated phase diagram of the bulk system, where we applied the mapping formulas (6) and (8) (empty symbols). $\diamond$: the estimated critical point at $\eta_{c,\mathrm{vl}} = 0.250(5)$ and $T^*_{c,\mathrm{vl}} = 0.346(5)$, $\triangle$: the mapped metastable fluid-fluid coexistence line, $\circ$: the mapped percolation line and $\triangledown$: the mapped fluid branch of the fluid-crystal coexistence line. Our present results for the percolation threshold are indicated by filled symbols. All dotted lines are guides to the eye.

finite (low η) and infinite (high η) clusters, respectively. Note that in both cases the clusters are *transient* in character, since there are no permanent bonds in our system.

According to Fig. 1, the lowest temperature $T^* = 0.5$, for which we investigated the percolation transition, lies near or even within the metastable region between fluid and solid states. Therefore we carefully examined the packing fraction and configurations generated during each GCMC run in order to guarantee that we average only in one phase. In particular, we analyzed the structure in terms of the radial distribution function $g(r)$. In Fig. 2 we show $g(r)$ together with the cavity function $\gamma(r) = g(r)e^{-u_{\mathrm{SW}}(r)/k_BT}$ of the bulk system at $T^* = 0.5$ at three packing fractions below, at and above the critical packing fraction for percolation η_c, which will be defined in Sec. IV. Since $g(r)$ and $\gamma(r)$ show no indication of any long rang order, we may conclude that we are indeed in the fluid phase.

III. COMPUTATIONAL DETAILS

To investigate the percolation behavior, we carried out standard GCMC simulations.[33] For the bulk system calculations have been performed at several reduced temperatures $T^* = 0.5, 1.0, 1.5, 2.0$. For the confined system we considered one fixed temperature, $T^* = 0.5$, and several wall distances ranging from $L_z = 1.5\sigma$ to $L_z = 10.0\sigma$. The sys-

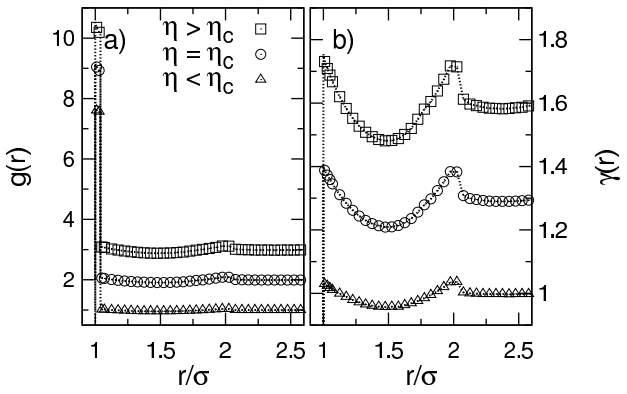

Figure 2. a) Radial distribution function $g(r)$ and b) cavity function $\gamma(r)$ at $T^* = 0.5$ for packing fractions below, at and above the percolation threshold [$\eta \approx 0.1$ ($\square$), $\eta = \eta_c \approx 0.23$ ($\bigcirc$) and $\eta \approx 0.3$ ($\triangle$)]. To improve the visibility, the graphs for $\eta = \eta_c$ ($\eta > \eta_c$) are shifted upwards by 1.0 (2.0) in a) and by 0.3 (0.6) in b). Dotted lines are guide to the eye.

tems are equilibrated by performing at least 10^5 GCMC cycles, where each cycle consist on $\langle N \rangle$ single particle displacement, insertion or deletion attempts, with $\langle N \rangle$ being the average number of particles in the system. Ensemble averages are obtained by analyzing at least 10^5 equilibrium configurations, separated by 80 cycles. With this choice of parameters the energy autocorrelation function between two averaging events is close to zero in all cases.

To determine the percolation threshold we performed at least four simulation runs at different basis lengths L for each system, where we have $L_x = L_y = L_z = L$ for the bulk system and $L_x = L_y = L > L_z$ for the slit-pore system. In each series, we chose the smallest L such that $\langle N \rangle \approx 500$ at $\eta = 0.1$. The largest systems we investigated contained about to 30000 particles.

An important aspect of any simulation study targeting percolation properties concerns the definition of clusters. Here we use a simple configurational criterion. Since we are dealing with a square-well model, two particles at positions $\boldsymbol{r}_i$ and $\boldsymbol{r}_j$ are unambiguously defined as connected if their distance is within the attractive well of the pair potential, i. e., $r_{ij} < \lambda$. The resulting configurational clusters may be considered as "percolated" if they are connected to their own periodic image.[15,34] In the 3D (bulk) system, we allow for percolation in any of the three spatial directions. The slit-pore system, on the other hand, is periodic only in the x- and the y-direction. Hence percolation can only occur in these two dimensions (2D). The whole system is considered as percolated if at least one percolating cluster exists.

To identify clusters and check for percolated configurations in our continuous model system, we implemented an algorithm as described in Ref. 15.

IV. ANALYSIS OF THE PERCOLATION TRANSITION

A. Determination of the percolation threshold

The purpose of this section is to outline our approach to determine the percolation threshold. Indeed, the definition of percolation itself is not unique in the literature. It depends on the system to be investigated, the definition of a percolated state and the definition of bonds.[1,14,35] This may lead to incompatible results for a single system. On the other hand, the definition of the percolation *threshold* is much clearer, at least for lattice systems. There one typically considers the probability p of finding a given lattice site occupied. The threshold p_c is then defined by the following criterion, that "for p above p_c one percolating network exists; for p below p_c no percolating network exists."[36]

We now have to clarify which quantity in our continuous system should play the role of the control variable p. Since we perform GCMC simulations, a natural control variable would be the activity (or the chemical potential, respectively). Here we prefer to use the (average) packing fraction η due to the obvious analogy between η and the occupancy of lattice sites.[15]

To determine the percolation threshold η_c, we examine the probability $\Pi(\eta, L)$ of finding a spanning cluster in a given system (3D or slit-pore) with a characteristic length L at packing fraction η. This probability, which depends on the system size L and the packing fraction η, can be calculated via an ensemble average of a test function $\pi(\{\boldsymbol{r}_k\}, L)$

$$\Pi(\eta, L) = \langle \pi(\{\boldsymbol{r}_k\}, L) \rangle \,, \tag{9}$$

where $\pi(\{\boldsymbol{r}_k\}, L) = 1$ if the configuration defined by $\{\boldsymbol{r}_k\}$ has one spanning cluster and 0 if all clusters are finite. It is commonly assumed (not rigorously proven) that $\Pi(\eta, L)$ fulfills a single-variable scaling law[1,36] of the form

$$\Pi\left(\eta, L\right) = \tilde{\Pi}\left(x\right) = \tilde{\Pi}\left((\eta - \eta_c) L^{1/\nu}\right). \tag{10}$$

The ansatz (10) involves the percolation threshold η_c, the critical exponent ν to be defined later [see Eq. (23)] and the master curve $\tilde{\Pi}(x)$, which is assumed to be unique for each set

of parameters. To obtain an accurate estimate of η_c we employ the following strategy (for a more detailed description see Ref. 1).

We first note that the probability $\Pi(\eta, L)$ is expected to have a sigmoidal shape with $\Pi(0, L) = 0$ and $\Pi(\eta \to \eta_{\rm cp}, L) = 1$, where $\eta_{\rm cp} = \sqrt{2}\pi/3 \approx 0.74$ is the packing fraction at close-packing (cp). Given this shape, the first derivative of $\Pi(\eta, L)$ with respect to η is a function with a peak at the packing fraction characterizing the steepest ascent of $\Pi(\eta, L)$. This feature, combined with the fact that $\partial\Pi/\partial\eta$ is normalized to one, allows us to define an average density $\eta_{\rm av}$ according to

$$\eta_{\rm av}(L) = \int_0^{\eta_{\rm cp}} d\eta\, \eta \frac{\partial \Pi}{\partial \eta}. \tag{11}$$

Furthermore, we can define the standard deviation $\Delta_{\rm av}$ via

$$\Delta_{\rm av}^2(L) = \int_0^{\eta_{\rm cp}} d\eta\, (\eta - \eta_{\rm av})^2 \frac{\partial \Pi}{\partial \eta}. \tag{12}$$

Using Eq. (10) to substitute $\tilde{\Pi}$ for Π and writing $\eta = x\, L^{-1/\nu} + \eta_c$, we obtain from Eq. (11) the linear dependence

$$\eta_{\rm av} = A\, L^{-1/\nu} + \eta_c \tag{13}$$

where A is a constant. Applying similar arguments to Eq. (12) results in

$$\Delta_{\rm av} \propto L^{-1/\nu}. \tag{14}$$

Combining Eqs. (13) and (14) finally yields the expression

$$\eta_{\rm av} - \eta_c \propto \Delta_{\rm av}. \tag{15}$$

Thus, Eq. (15) predicts a *linear* relationship between $\eta_{\rm av}$ and $\Delta_{\rm av}$, with η_c playing the role of an y-intercept. We have used this relationship to obtain the percolation threshold. In order to actually calculate $\eta_{\rm av}$ and $\Delta_{\rm av}$, we have fitted the numerical data for $\Pi(\eta, L)$ according to the expression (see Ref. 15)

$$f(x; \{a_i\}) = 1 + \tanh\left(\sum_{i=0}^{5} a_i x^i\right) \tag{16}$$

involving the six fitting parameters $\{a_i\}$. Some representative numerical results for $\eta_{\rm av}$ as function of $\Delta_{\rm av}$ are given in Fig. 3a) and c). In Fig. 3a) we consider bulk systems at various reduced temperatures. Clearly, the data points for $\eta_{\rm av}$ form nearly perfect straight

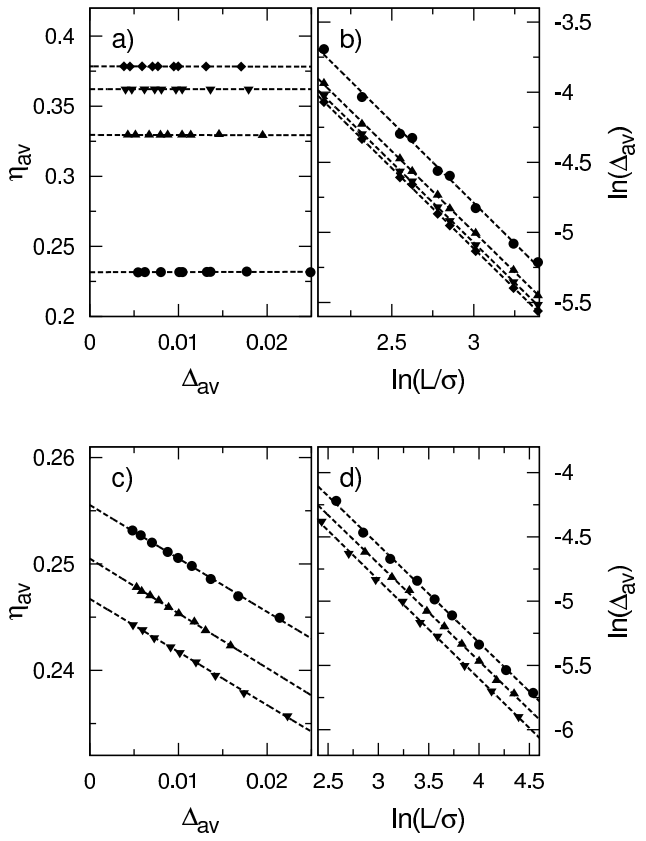

Figure 3. Upper panel: Determination of the percolation threshold and the exponent ν for bulk systems of temperatures $T^* = 0.5$ (•), 1.0 (▲), 1.5 (▼) and 2.0 (♦). The plots show a) the average packing fraction $\eta_{\rm av}$ as function of the standard deviation $\Delta_{\rm av}$ and b) the (logarithm of) the standard deviation as function of system size. The dashed lines are obtained from least square fit. From a) the percolation threshold follows as the intercept on the y-axis [see Eq. (15)]. From b), the exponent ν follows as the slope of the lines [see Eq. (14)]. Lower panel: Analog to the upper panel, but for slit-spore systems at temperature $T^* = 0.5$ and $L_z = 3.0\sigma$ (•), 3.5σ (▲) and 4.0σ (▼).

lines, consistent with Eq. (15), which allows us to extract the percolation threshold density η_c easily. The averaged gradient A of these nearly parallel lines is essentially zero, $A = -0.002 \pm 0.005$. The results for η_c at the four temperatures investigated are plotted in Fig. 1. Figure 3c) shows the same type of data for the slit-pore systems with various wall separations. The results reflect a very good accuracy of the approach again. Here, the averaged gradient is close to $-1/2$ (i. e., $A = -0.505 \pm 0.005$). The resulting percolation thresholds for the confined systems are further discussed in Sec. IV B.

In a similar fashion, we can use Eq. (14) to obtain the critical exponent ν [which is involved

in the scaling law (10)]. To this end we plot in Fig. 3b) and d) the standard deviation $\Delta_{\rm av}$ as a function of the system size in a double-logarithmic representation. Again, we find that the relationship predicted by Eq. (14) is essentially perfectly fulfilled for both, bulk and slit-pore systems. Finally, having determined η_c and ν, we can test the underlying scaling assumption for $\Pi(\eta, L)$ given in Eq. (10). We have done this test for all systems investigated. Results for bulk and slit-pore systems at $T^* = 0.5$ are shown in Fig. 4. For both cases the

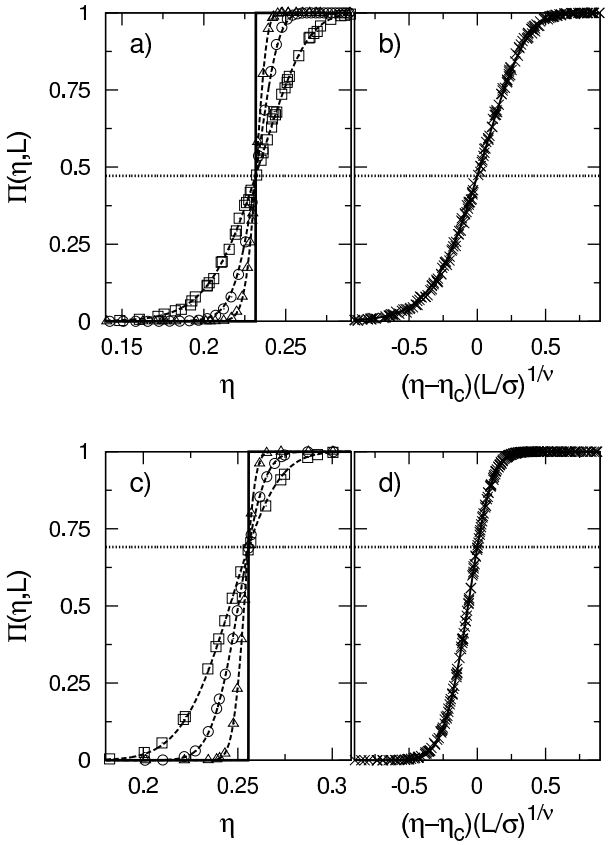

Figure 4. Upper panel: Percolation probability $\Pi(\eta, L)$ of the bulk system at $T^* = 0.5$. a) Simulation data for three system sizes $L = 8.06\sigma$ ($\square$), 16.12σ ($\bigcirc$) and 29.7σ ($\triangle$). The dashed lines are obtained via least square fits of Eq. (16). The bold solid line denotes the assumed limiting shape for $L \to \infty$. The dotted line marks $\Pi(\eta_c, L)$. b) Shifted and scaled simulation data ($\times$) for all nine investigated system sizes, ranging between $L = 8.06\sigma$ and $L = 29.7\sigma$. The bold solid line denote the assumed shape of the master curve $\tilde{\Pi}(x)$ as obtained from a least square fit of Eq. (16). Lower panel: Same as the upper panel, but for a slit-pore system at $T^* = 0.5$, $L_z = 3.0\sigma$ and three system sizes $L = 13.21\sigma$ ($\square$), 29.54σ ($\bigcirc$) and 93.42σ ($\triangle$).

data obtained for different system sizes indeed falls on one master curve, consistent with the

theory. Numerical values for the exponent ν are given in the subsequent Sec. IV B.

B. Further critical exponents

In addition to the exponent ν mentioned in Sec. IV A, we have determined three more critical exponents. These are the two Fisher exponents (FE) $\tau_{\rm FE}$ and $\sigma_{\rm FE}$, and the fractal dimensionality D, which are related to the cluster size distribution, $n(s;\eta)$, and the distribution of radii of gyration, $R(s;\eta)$.[4,37] Thus, the exponents $\tau_{\rm FE}$, $\sigma_{\rm FE}$, and D have geometric (rather than thermodynamic) character. Nevertheless, one can show[4] that these exponents are linked to thermodynamic quantities such as the pressure via scaling relations. This link can be made in the framework of the fisher droplet model[38,39] of an ideal cluster gas. Here we focus on relationships between the "geometric" exponents. The cluster size distribution is defined as the average number of *finite* clusters of size s at packing fraction η. Close to the percolation threshold, this quantity displays power-law behavior, i. e.,

$$n(s;\eta_c) \sim s^{-\tau_{\rm FE}} \tag{17}$$

as $s \to \infty$. Equation (17) defines the Fisher exponent $\tau_{\rm FE}$. The second Fisher exponent, $\sigma_{\rm FE}$, appears when we consider the k-th moment m_k of $n(s;\eta)$

$$m_k(\eta) = \sum_{s=0}^{\infty} s^n n(s;\eta). \tag{18}$$

Using Eq. (17), we find that m_k fulfills the power law

$$m_k(\eta) \propto |\eta - \eta_c|^{-(k-\tau+1)/\sigma_{\rm FE}}. \tag{19}$$

We now consider the distribution of radii of gyration $R(s;\eta)$. For a fixed size s, the radius of gyration of a single cluster is defined as the averaged mean squared distance of the particles relative to the cluster's center of mass (CM) position $\boldsymbol{r}_{\rm CM} = \sum_{i=1}^{s} \boldsymbol{r}_i/s$. This implies[35]

$$R(s;\eta) = \sqrt{\left\langle \frac{1}{s}\sum_{i=1}^{s} (\boldsymbol{r_i} - \boldsymbol{r}_{\rm CM})^2 \right\rangle}. \tag{20}$$

Close to the percolation threshold, the critical behavior of this distribution is given through the power law

$$R(s;\eta_c) \sim s^{1/D} \tag{21}$$

as $s \to \infty$. We introduced the fractal dimensionality D as the critical exponent of the gyration radius. The distribution $R(s;\eta)$ also allows us to define the correlation length characterizing the system,

$$\xi = \sqrt{2\frac{\sum_{s=0}^{\infty} R(s;\eta)s^2 n(s;\eta)}{\sum_{s=0}^{\infty} s^2 n(s;\eta)}}. \tag{22}$$

The correlation length diverges at the percolation threshold as[1,37]

$$\xi \propto |\eta - \eta_c|^{-\nu}, \tag{23}$$

which defines the exponent ν already mentioned in Sec. IV A. Finally, using the definition (22) and the power-law relations (19), (21) and (23) one can find the scaling relation

$$D = \frac{1}{\sigma_{\mathrm{FE}}\nu}, \tag{24}$$

which we use to determine the fisher exponent σ_{FE} from the knowledge of ν and D. The power laws given in Eqs. 17 and 21 hold only in the limit $s \to \infty$. In fact, for the cluster size distribution the exponent τ_{FE} determines only the leading term in a series expansion of the form

$$n(s;\eta_c) \sim s^{-\tau_{\mathrm{FE}}}(1 + A\, s^{-\Omega} + \ldots). \tag{25}$$

In Eq. (25) the critical exponent Ω is introduced as a first order correction to the scaling ansatz.[40]

To treat the system of finite size, we performed simulations for each analyzed slit-pore system, using the appropriate values of the critical activity to obtain η_c in each case. We prepared the raw data by "logarithmic binning" of the distributions $n(s;\eta_c)$ and $R(s;\eta_c)$. To this end, we average the distributions over intervals $I_n = [b_0\frac{b^{n+1}-1}{b-1}, b_0\frac{b^{n+2}-1}{b-1}]$, where the width b_n of each I_n grows as $b_n = b_0 b^n$ and hence produces equally spaced nodes on a logarithmic axis.[41] This introduces some arbitrariness via the choice of b. For practical reasons we have to choose b such that the noise-level of the averaged distributions is sufficiently small. On the other hand, we must be careful not to obscure the main tendencies. We then plot the averaged data in a double-logarithmic representation and approximate the local slope by difference quotients. For sufficiently large s we expect to observe a clear plateau. Indeed, from the definition of the critical exponents τ_{FE} and D in Eqs. (21) and (25) it follows that

$$\lim_{s\to\infty} n'(s;\eta_c) = -\tau_{\mathrm{FE}} \tag{26}$$

and analogously

$$\lim_{s\to\infty} R'(s;\eta_c) = \frac{1}{D}. \tag{27}$$

Here, $f'(s) = \partial \ln f(s)/\partial \ln s$ (where $f = n$ or R). In Fig. 5 we show exemplary data for the

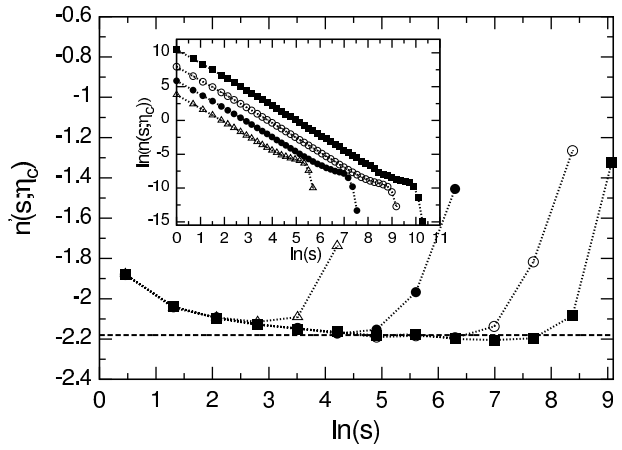

Figure 5. Local slope $n'(s;\eta_c)$ of the double-logarithmic representation of the cluster-size distribution $n(s;\eta_c)$ (inset) for the bulk system at reduced temperature $T^* = 0.5$ and four system sizes $L = 9.35\sigma$ (△), 18.71σ (•), 37.42σ (○) and 55.13σ (■). The logarithmic-binning (See Sec. IV B) is done using $b = 2$ for the local slope and $b = 1.3$ for the inset. The dashed line denotes the value of the fisher exponent τ_{FE} for 3D random percolation.

functions $n'(s;\eta_c)$ and $n(s;\eta_c)$ (inset) for the bulk system at $T^* = 0.5$ for four system sizes. For the largest system, $L = 55.13\sigma$, we can indeed clearly identify a plateau. The deviations for large s are due to the limitations in the system size. For clusters with a characteristic length approaching the system length L, the probability of being *not* percolated has to drop rapidly, since percolated clusters do not contribute to the distributions.

In Fig. 6 we show, again for the bulk system, the two functions $n'(s;\eta_c)$ and $R'(s;\eta_c)$ at four different temperatures (and the largest L considered). All curves exhibit a plateau, which is reached the faster (in terms of the cluster size s) the higher T^*. The important point, however, is that the plateau heights are essentially independent of T^*. This means that the exponents τ_{FE} and D [see Eqs. (26) and (27)] extracted from our simulations may be considered as "universal", that is, not influenced by the temperature. Furthermore, the observation that the temperature does not affect the value of the critical exponents but the speed of convergence may offer an explanation for the observed temperature dependence of the critical exponents for more complex interaction models.[15] An overview of our results for

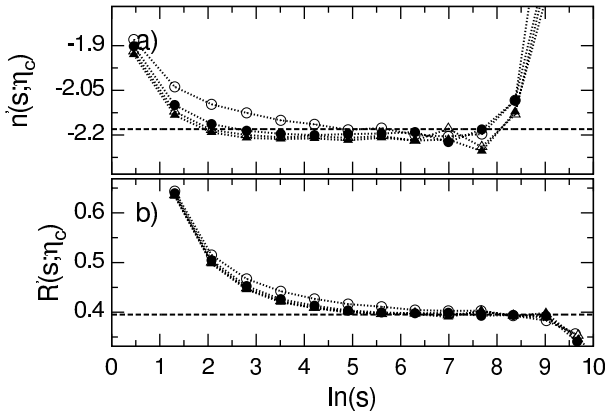

Figure 6. Logarithmic slopes $n'(s;\eta_c)$ a) and $R'(s;\eta_c)$ b) for the bulk system at the four investigated temperatures $T^* = 0.5\,(\circ)$, $1.0\,(\bullet)$, $1.5\,(\triangle)$ and $2.0\,(\blacktriangle)$ directly at the corresponding percolation thresholds. The results are for the largest system size investigated for the bulk system ($L = 55.13\sigma$). The bold dashed lines denote the values for the critical exponent $\tau_{\rm FE}$ (part a)) and D (part b)) for 3D random percolation.

the bulk system is given in Tab. I. It is visible that the critical exponents $\tau_{\rm FE}$ and D are

Table I. Critical parameters for the bulk system.

T^*	η_c	$\Pi_{\rm c}$	ν	D	$\tau_{\rm FE}$	$\sigma_{\rm FE}$
0.5	0.23165(5)	0.47	0.86	2.48	2.19	0.47
1.0	0.32960(5)	0.44	0.87	2.51	2.20	0.46
1.5	0.36337(5)	0.46	0.86	2.52	2.21	0.46
2.0	0.3800(3)	0.48	0.88	2.51	2.21	0.45
3D r. p.[a]	-	-	0.88	2.53	2.18	0.45

[a] Literature values for the critical exponents relevant in 3D random percolation (r. p.).[1,42]

close to those obtained for 3D random percolation (see horizontal lines in Fig. 6).

We now turn to the slit-pore systems. In Fig. 7 we present $n'(s;\eta_c)$ and $R'(s;\eta_c)$ as functions of $\ln(s)$ for six values of the wall separation L_z. The convergence of the data (as characterized by the appearance of a plateau) strongly depends on L_z. Specifically, the larger L_z, the larger cluster sizes are needed before n' and R' reach a plateau. Moreover, in some cases, there is no clear plateau at all (see e.g. data for n' at $L_z = 10\sigma$). For the other cases, the observed plateau heights are close to those predicted by 2D random percolation

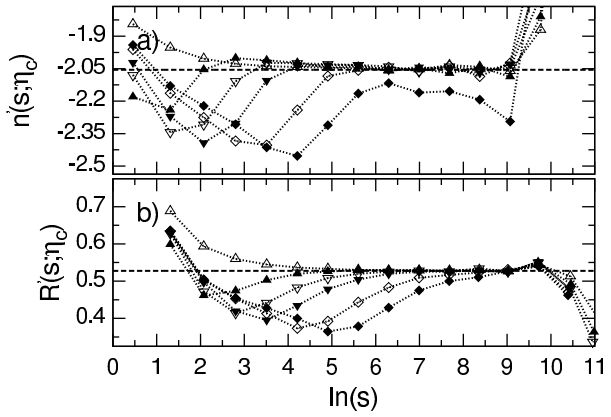

Figure 7. Same as Fig. 6, but for slit-pore systems at temperature $T^* = 0.5$. To improve the visibility, only the results for $L_z = 1.5\sigma$ (△), 3.0σ (▲), 4.0σ (▽), 5.0σ (▼), 7.5σ (◇), and 10.0σ (◆) are shown. The results are obtained for the largest system size we investigated in each case. The bold dashed lines denote the values for the critical exponent τ (part a)) and D (part b)) for 2D random percolation.

theory. The latter are summarized in Table II. An overview of our numerical data for the

Table II. Critical exponents for 2D random percolation.

	ν^{2D}	D^{2D}	τ_{FE}^{2D}	σ_{FE}^{2D}
exact	$\frac{4}{3}$	$\frac{91}{48}$	$\frac{187}{91}$	$\frac{36}{91}$
numerical	1.33	1.90	2.05	0.40

exponents τ_{FE}, D, ν, and σ_{FE} as functions of the wall separation is given in Fig. 8. The graphs also indicate the corresponding literature values for 2D and 3D random percolation. Within the entire range investigated ($L_z < 10\sigma$) the fractal dimensionality is very close to the 2D value, and a similar consistency is found for the exponent of the correlation length, ν, and the exponent σ_{FE}. Compared to that, the data for τ_{FE} are more scattered, consistent with what is seen in Fig. 7a).

As far as the slit-pore systems are considered, there are (at least) two sources of errors which come into play. The larger the wall separation L_z, the larger cluster sizes s are needed to observe a clear plateau. Hence, our system size may still be chosen too small. Furthermore, we can observe real 2D behavior only if we know the percolation thresholds η_c with sufficient accuracy. We expect the error tolerance of η_c to decrease with increasing

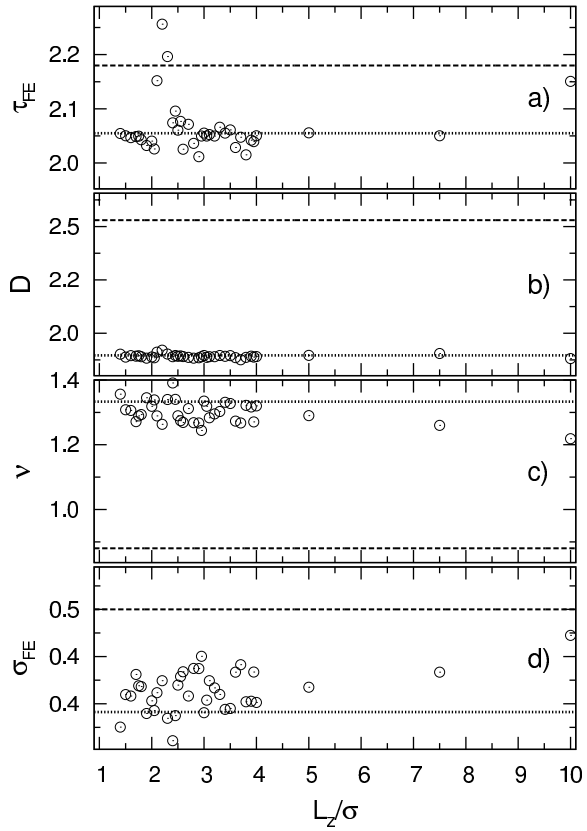

Figure 8. Estimated critical exponents τ_{FE} (a), D (b), ν (c) and σ_{FE} (d) for the slit-pore systems at $T^* = 0.5$ as functions of the wall distances L_z. The exponent σ_{FE} is deduced from Eq. (24). The lines denote the values for 3D (dashed) and 2D (dotted) random percolation.

wall distance L_z[43,44] and in this spirit, we only measure effective exponents. At $L_z \approx 2\sigma$ we observe, especially for the fisher exponent τ_{FE}, strong deviations from the 2D value of random percolation. We suppose this irregularity to occur due to the vicinity a freezing transition, which position in the phase diagram is known to depend on the wall separation[45] (see Fig. 9 a).

C. Confinement-induced shift of the percolation threshold

So far we have focused on the critical exponents characterizing the percolation transition. We now consider, for the confined systems, the actual location of this transition in the phase diagram. To this end, we depict in Fig. 9 a) the critical packing fraction η_c and in Fig. 9 b) the corresponding chemical potential of the percolation threshold for various wall separations. For comparison, we also show the freezing line of a pure hard sphere system confined between

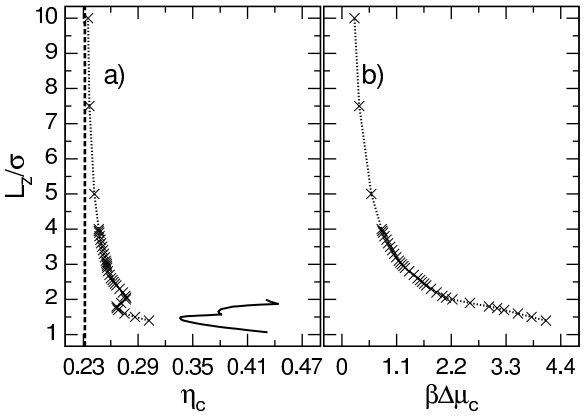

Figure 9. Relation between the percolation threshold and the wall separation for the slit-pore systems at $T^* = 0.5$. Specifically, part a) shows the packing fraction $\eta_c(L_z)$, while b) shows the difference of the chemical potential to the corresponding bulk value $\beta\Delta\mu_c = \beta(\mu_c(L_z) - \mu_c(\infty))$. The dotted line is a guide to the eye. The dashed line denotes the value of the bulk threshold at $\eta_c(\infty)$ [see Tab. II]. The solid line marks the freezing line of a pure hard sphere system which is confined between two hard walls (data taken from Fig. 4 of Ref. 45).

two parallel, hard walls (solid line) in Fig. 9 a). The data was taken from Fig. 4 of Ref. 45. The pure hard-sphere system corresponds to our model at large temperatures, i. e., $T^* \to \infty$.

Inspecting Fig. 9 a) we find that with decreasing L_z the percolation threshold η_c increases until $L_z \approx 2\sigma$. At even smaller wall separations the relation between η_c and L_z becomes non-monotonic.

In the following we focus on the behavior observed for $L_z \gtrsim 2\sigma$, i. e., the shift of the percolation threshold with respect to the bulk values. In particular, we give an argument which has successfully been used to explain the shifts of the gas-liquid critical point in a slit-pore confinement.[43,44] The most remarkable point of this argument is that it does not rely on any detailed information of the underlying system of interest, but only on the dimensionality and the interaction range. In Sec. IV A we have derived the percolation thresholds for fixed L_z by performing a finite-size analysis with respect to the lateral dimensions $L_x = L_y = L$ [see Eq. (11)], i. e., we have let $L \to \infty$. This way we obtaine the percolation threshold η_c, which still depends on the remaining length L_z. We now see that, for large L_z, the behavior upon further increasing L_z towards infinity is the same as that seen for $L \to \infty$ for the bulk system.[46] In other words, we assume that a relation similar to Eq. (11) should also hold for $\eta_c(L_z)$. Moreover, we assume that, for sufficiently large L_z, the corresponding exponent ν

should be that of the 3D system, $\nu^{3D} \approx 0.88$. These considerations lead to

$$\Delta\eta_c^*(L_z) = \eta_c^*(L_z) - \eta_c^*(\infty) \propto L_z^{-1/\nu_{3D}}. \tag{28}$$

In Eq. (28), $\eta_c^*(L_z)$ denotes the packing fraction of a bulk system which is in chemical equilibrium with a slit-pore system of width L_z (and at average packing fraction η_c). Indeed, using this notation, $\eta_c^*(\infty)$ is identical to the percolation threshold of the bulk system η_c^{3D} at $T^* = 0.5$.

Since we consider our system to be above the gas-liquid critical temperature the density is a continuous function of the chemical potential. Hence we may write, for small deviations $\Delta\mu_c(L_z)$ from the bulk value $\mu_c(\infty)$ (i. e., sufficiently large L_z),

$$\Delta\mu_c(L_z) = \mu_c(L_z) - \mu_c(\infty) \propto L_z^{-1/\nu_{3D}}. \tag{29}$$

In Fig. 10 we compare our numerical results for $\Delta\eta_c^*(L_z)$ and $\Delta\mu_c(L_z)$ with the predictions

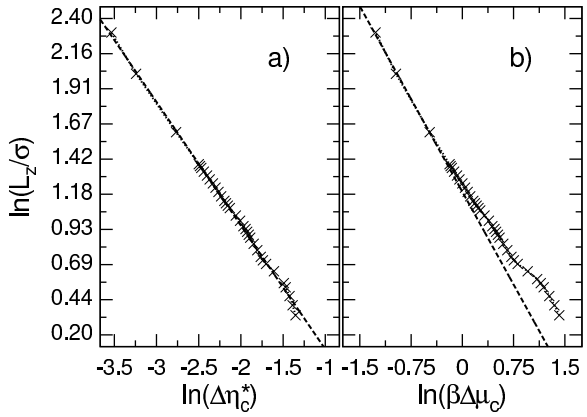

Figure 10. Scaling of the confinement-induced shifts of the percolation threshold at $T^* = 0.5$. The shifts are given in terms of a) the corresponding densities of a bulk system in equilibrium with the slit-pore $\Delta\eta_c^*$, and b) the change of the chemical potential $\beta\Delta\mu_c$. The gradient of the straight lines is set to $-1/\nu_{3D}$ as required by Eqs. (28) and (29).

of Eqs. (28) and (29), by plotting a straight line (dashed) with a fixed slop $-1/\nu_{3D}$ together with the data. From Fig. 10 a) we find that Eq. (28) is at least qualitatively fulfilled even for the smallest wall distances investigated. Moreover, the shift of the chemical potential shown in Fig. 10 b) is sufficiently well described by Eq. (29) for $L_z \gtrsim 4\sigma$. For not too small L_z we can thus conclude that the confinement-induced shift of the percolation threshold η_c can successfully be described by Eqs. (28) and (29). Hence we have shown that the same

scaling arguments, which are usually applied to the shift of the gas-liquid critical point in a slit-pore confinement,[43,44] also apply to the shift of the percolation threshold.

V. CONCLUSION

Based on grand-canonical MC simulations and a finite-size-scaling analysis we have studied the percolation behavior of a model colloidal suspension with an ultra-short range of attraction in three dimensions and in slit-pore geometries. Our aim in this study was twofold: On the one hand, we wanted to provide "fresh" data on the somewhat controversial issue of the universality of critical exponents of percolation in 3D continuous systems. On the other hand, we aimed to explore the impact of spatial confinement on the percolation transition; a question which was so far essentially unexplored. The model we have studied consists of hard spheres with a square-well attraction extending over (only) four percent of a particle diameter. As a result, the bulk systems lacks a stable liquid phase (i. e., the vapor-liquid-transition predicted by a mapping procedure from the Baxter model is metastable), and the only true transition within the fluid phase is the percolation transition. Using a finite size analysis we have first determined the percolation threshold, η_c, of the bulk system at four temperatures above the critical temperature. Consistent with an earlier simulation study of a similar square-well fluid (yet with a significantly larger attraction range),[26] we found that η_c increases with increasing reduced temperature and slowly converges to the limiting value determined by a pure hard sphere system (i. e., the limit $T^* \to \infty$ of our model).

Regarding the critical exponents of the 3D percolation transition, however, our present results differ from the earlier ones in Ref. 14. In that study, the exponent ν of the correlation length was found to depend on the temperature, specifically ν decreased with T^*. This led the authors of Ref. 14 to conclude that the exponent is "non-universal". Contrary to these results, our present data reveal no systematic dependence of ν on the temperature; instead, the numerical values of ν fluctuate around the corresponding value predicted by 3D random percolation theory. The question remains whether this contradiction could be due to the different range of attraction considered in our study and in Ref. 14.

In addition to ν, we also studied the exponents τ_{FE} and D governing the cluster size distribution $n(s;\eta_c)$ and the radii of gyration, respectively. For sufficiently large system sizes, we find these exponents to be independent on the temperature and their magnitude

to be very close to those predicted by 3D random percolation theory again.

To get an insight of the impact of spatial confinement, we performed GCMC simulations at several wall separations in the range $1.5\sigma \leq L_z \leq 10\sigma$ at fixed reduced temperature $T^* = 0.5$. All of these confined systems displayed a clear percolation transition, with the percolation value of the chemical potential (and also the resulting η_c) being shifted relative to its bulk value (at $T^* = 0.5$).

Specifically, upon decreasing L_z from infinity (bulk limit), we find a *monotonic* increase of η_c until the wall separation comes close to the 2D limit ($L_z/\sigma \gtrsim 2$). Moreover, in this range of wall separations the shift of η_c can be mathematically described by simple scaling arguments similar to those applied in the framework of cross-over scaling for vapor-liquid critical points in slit pores.[43,44] In addition to the percolation threshold, we have also analyzed the critical exponents for the slit-pore systems (see Fig. 8). The exponent ν is always close to the value predicted by 2D random percolation theory and shows no systematic dependence on L_z. Regarding the other exponents, we have found that convergent results (extractable from a plateau in the derivatives of the relevant distribution functions) are generally the harder to obtain the larger the wall separation is. Nevertheless, in the cases where we could extract reliable data, the exponents are comparable to those of 2D random percolation.

We thus conclude that the percolation transition of colloidal systems with ultra-short ranged interactions falls into the universality class of random percolation, the only important factor being *that* the spatial dimension along which the system is finite (3D or 2D).

From an experimental and applicational point of view one is often interested in the consequences of percolation, such as a strong increase of the macroscopic conductivity, rather than in the transition itself. In this context, we expect our results for the confined systems to be particularly relevant, since real experimental situations often involve confinement. We note that the model considered here is appropriate for a broad range of colloidal suspensions involving depletion "agents" which cause the short-range attraction. From a more conceptual point of view, it is interesting that colloidal systems with such "sticky" interactions — at least in 3D — can not only form percolated static structures, but an also display non-trivial dynamical behavior such as gelation and glass formation.[11,13,47] In particular, for spatially confined systems the interplay between gelation and percolation is essentially unexplored. These issues will be subject of future studies.

REFERENCES

[1]D. Stauffer and A. Aharony, *Introduction to percolation theory* (Taylor & Francis, 2003).

[2]M. E. Fisher and B. U. Felderhof, Ann. Phys. (N. Y., NY, U. S.) **58**, 217 (1970).

[3]M. E. Fisher and B. U. Felderhof, Ann. Phys. (N. Y., NY, U. S.) **58**, 176 (1970).

[4]N. Sator, Phys. Rep. **376**, 1 (2003).

[5]R. H. J. Otten and P. van der Schoot, Phys. Rev. Lett. **108**, 088301 (2012).

[6]R. H. J. Otten and P. van der Schoot, J. Chem. Phys. **134**, 094902 (2011).

[7]R. H. J. Otten and P. van der Schoot, Phys. Rev. Lett. **103**, 225704 (2009).

[8]T. Schilling, S. Jungblut, and M. A. Miller, Phys. Rev. Lett. **98**, 108303 (2007).

[9]E. Zaccarelli, P. J. Lu, F. Ciulla, D. A. Weitz, and F. Sciortino, J. Phys.: Condens. Matter **20**, 494242 (2008).

[10]Y. Duda, J. Chem. Phys. **130**, 116101 (2009).

[11]L. Rovigatti, J. Russo, and F. Sciortino, Soft Matter **8**, 6310 (2012).

[12]F. Romano and F. Sciortino, Nat. Mater. **10**, 171 (2011).

[13]F. Sciortino and E. Zaccarelli, Curr. Opin. Solid State Mater. Sci. **15**, 246 (2011).

[14]J. Skvor, I. Nezbeda, I. Brovchenko, and A. Oleinikova, Phys. Rev. Lett. **99**, 127801 (2007).

[15]J. Skvor and I. Nezbeda, Phys. Rev. E **79**, 041141 (2009).

[16]J. Skvor and I. Nezbeda, Mol. Phys. **109**, 133 (2011).

[17]P. J. Lu, E. Zaccarelli, F. Ciulla, A. B. Schofield, F. Sciortino, and D. A. Weitz, Nature **453**, 499 (2008).

[18]B. Bharti, J. Meissner, and G. H. Findenegg, Langmuir **27**, 9823 (2011).

[19]E. H. A. de Hoog, W. K. Kegel, A. van Blaaderen, and H. N. W. Lekkerkerker, Phys. Rev. E **64**, 021407 (2001).

[20]W. K. Wijting, N. A. M. Besseling, and M. A. C. Stuart, Phys. Rev. Lett. **90**, 196101 (2003).

[21]S. Asakura and F. Oosawa, J. Polym. Sci. **33**, 183 (1958).

[22]N. Asherie, A. Lomakin, and G. B. Benedek, Phys. Rev. Lett. **77**, 4832 (1996).

[23]M. Schmidt, A. Fortini, and M. Dijkstra, J. Phys.: Condens. Matter **16**, S4159 (2004).

[24]M. G. Noro and D. Frenkel, J. Chem. Phys. **113**, 2941 (2000).

[25]G. Foffi and F. Sciortino, Phys. Rev. E **74**, 050401 (2006).

[26]J. Largo, M. A. Miller, and F. Sciortino, J. Chem. Phys. **128**, 134513 (2008).

[27]R. J. Baxter, J. Chem. Phys. **49**, 2770 (1968).

[28]M. A. Miller and D. Frenkel, J. Phys.: Condens. Matter **16**, S4901 (2004).

[29]G. Foffi and F. Sciortino, J. Phys. Chem. B **111**, 9702 (2007).

[30]E. Zaccarelli, J. Phys.: Condens. Matter **19**, 323101 (2007).

[31]M. A. Miller and D. Frenkel, Phys. Rev. Lett. **90**, 135702 (2003).

[32]G. Foffi, G. D. McCullagh, A. Lawlor, E. Zaccarelli, and K. A. Dawson, Phys. Rev. E **65**, 031407 (2002).

[33]M. P. Allen and D. J. Tildesley, *Computer Simulation of Liquids* (Clarendon Press, Oxford, 1987).

[34]T. Edvinsson, P. J. Rasmark, and C. Elvingson, Mol. Simul. **23**, 169 (1999).

[35]D. M. Heyes and J. R. Melrose, Mol. Phys. **68**, 359 (1989).

[36]D. Stauffer, Phys. Rep. **54**, 1 (1979).

[37]A. Kapitulnik, A. Aharony, G. Deutscher, and D. Stauffer, J. Phys. A: Math. Gen. **16**, L269 (1983).

[38]M. E. Fisher, Rep. Prog. Phys. **30**, 615 (1967).

[39]M. E. Fisher, J. Appl. Phys. **38**, 981 (1967).

[40]R. M. Ziff, Phys. Rev. E **83**, 020107 (2011).

[41]S. Milojevic, J. Am. Soc. Inf. Sci. Technol. **61**, 2417 (2010).

[42]C. D. Lorenz and R. M. Ziff, Phys. Rev. E **57**, 230 (1998).

[43]R. L. C. Vink, A. De Virgiliis, J. Horbach, and K. Binder, Phys. Rev. E **74**, 031601 (2006).

[44]R. L. C. Vink, K. Binder, and J. Horbach, Phys. Rev. E **73**, 056118 (2006).

[45]M. Schmidt and H. Löwen, Phys. Rev. E **55**, 7228 (1997).

[46]J. Cardy, *Scaling and Renormalization in Statistical Physics* (Cambridge University Press, 1996) pp. 73–75.

[47]I. Saika-Voivod, H. M. King, P. Tartaglia, F. Sciortino, and E. Zaccarelli, J. Phys.: Condens. Matter **23**, 285101 (2011).